Received: 28 January 2020 | Revised: 5 May 2020 | Accepted: 5 May 2020

DOI: 10.1002/eng2.12196

RESEARCH ARTICLE

WILEY

Analysis of DGS filters using π-circuit model

Sambhav Malhotra[1] | **Mohammad Hashmi**[1,2]

[1]Department of Electronics Communication Engineering, IIIT Delhi, New Delhi, India

[2]School of Engineering Digital Sciences, Nazarbayev University, IIIT Delhi, Nur Sultan, Kazakhstan

Correspondence
Sambhav Malhotra, Department of Electronics Communication Engineering, IIIT Delhi, New Delhi 110020, India.
Email: sambhav14158@iiitd.ac.in.

Funding information
Nazarbayev University FDCRG, Grant/Award Number: SOE2019005: 110119FD4515

Abstract

The design and analysis of two defected ground structures (DGS)-based filters have been proposed in this article. The first is a multifrequency bandstop filter (BSF) which utilizes a semi-H defect in the ground plane. This structure is then prototyped on a Rogers 4350B substrate of overall size 45 mm × 15 mm with an external SMD capacitors employed to control the resonance of the circuit for the stopband frequencies of 433, 700, and 915 MHz. An equivalent π-circuit is modified to validate this multiband filter. The second filter is a combination of a BSF and bandpass filter in one structure. The filter operating with a controllable passband and stopband frequency is fabricated on Rogers 4350B lossy substrate. Two SMD capacitors are loaded in the filter structure to control the passband and stopband frequencies of the filter with a structure size of 20 mm x 20 mm. Finally, the equivalent circuit from the BSF is modified further to encompass the bandpass and bandstop frequency response of the proposed work.

KEYWORDS

multiband DGS, π circuit model, bandstop filter, bandpass filter

1 | INTRODUCTION

Defected ground structures (DGS) are introduced in order to improve the performance of microstrip circuits and components while minimizing the overall size of the design.[1-4] In a DGS, defects are introduced in the ground plane to improve the frequency response of the considered components . The geometry of this defect is selected such that it disturbs the surface current in the ground plane and helps in achieving the desired electromagnetic effect. The miniaturization, selectivity, bandwidth enhancement, and so on provided by the DGS has catapulted this as a key concept in the design of many high frequency circuits and components such as filters, power dividers, antennas, antenna arrays, and so on[5-8]

The recent literature is replete with reports of DGS-based bandstop filters (BSFs) and their usage in near-field wireless power transfer (WPT) systems.[9-13] In essence, performance of DGS-based filter plays a crucial role in regulating the power transfer efficiency of the WPT circuits and, therefore, there has been a great deal of research on this topic.[14-17] It has been established that the DGS filters used in the design of WPT systems can be simplified through equivalent circuit-based analysis. The equivalent circuit models of such filters are relatively simple in nature and do not consider the effects of the discontinuity present between the microstrip line and the defected ground plane. However, the report on the π- type equivalent circuit to model the DGS which looks into this concern to some extent[18] can be useful for the design of more

The work was financially supported in part through the Nazarbayev University FDCRG Number SOE2019005 (110119FD4515).

performance centric near-field WPT systems. This concept,[18] although very exciting, does not explore the use of external capacitors often required in WPT systems in tuning the frequency.

Furthermore, DGS concepts have also been abundantly used in the design of bandpass filters (BPFs).[19-24] These filters find wide range of applications in wireless systems.[25] There are generally two methods which generate a bandpass frequency response. One method is coupled resonators, which require two BSFs put back to back to generate a bandpass frequency response.[19-21] The second type is based around the use of a single DGS structure to get the bandpass frequency response by creating a coupling gap in the microstrip feed line.[22-24] Since, the structure of a filter should not take up too much space on a device, having two filters to generate a bandpass frequency response is considered suboptimal and therefore the second method is considered more exciting.[26-29] Once again, most of the reported equivalent circuit models fall short of covering various losses associated with the DGS.

Two different DGS structures are, therefore, explored in this article to facilitate the analysis of DGS-based filters by considering the apparent losses and discontinuity. The first is a triple-band DGS-based BSF using semi-H DGS which is analyzed and validated using an equivalent circuit model. It improves on the existing πcircuit model and proposes an approach to accommodate multiple bands. The second design focuses on the design of a passband and stopband frequency DGS filter using an H-shaped DGS with a coupling gap in the feed line. In both the cases, the presence of external SMD capacitor provides control over the achievable resonant frequency, enables good narrowband response, and reduces the size of the overall structure. Sections 2 and 3 are dedicated to the design and prototype validation of the multiband BSF. Subsequently, the Sections 4 to 6 improve on the proposed BSF circuit model for use in the design and analysis of a single-band BSF/BPF. Finally, Section 7 concludes the article.

2 | THEORETICAL ANALYSIS

2.1 | Design of triple-band filter

Three rectangular DGS resonators exhibiting bandstop characteristics are implemented in a cascaded fashion on a Rogers 4350B substrate, with the parameters ϵ_r=3.6, h_{sub}=1.524 mm and h_{copper}=35 μm,as shown in Figure 1 The top plane of the DGS resonator consists of 50 Ωmicrostrip feed line of length L_{MSL}andwidth W_{MSL}asdepicted in Figure 2.

The defects in the ground plane are connected to an excitation slot g, which houses the external SMD capacitors. These capacitors are loaded in the respective slots and along with the various sized defects combine to form bandstop responses at 433, 700, and 915 MHz. Following six parameters define the overall size of the defects:

1) *a and b* = length and width of defect 1
2) *c and d* = length and width of defect 2
3) *e and f* = length and width of defect 3

A thorough simulation is carried out in CST Microwave Studio and the relevant design parameters to conduct the simulation of the design of the BSF are given in Table 1. Furthermore, optimization of the structure is done to ensure

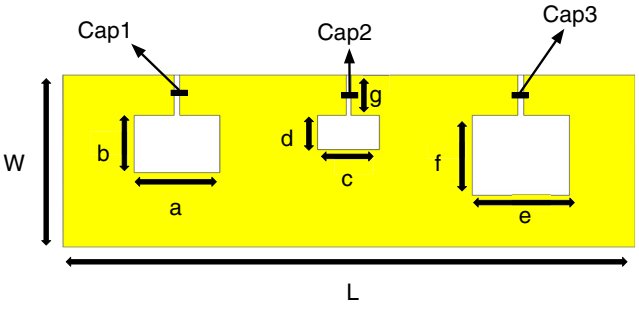

FIGURE 1 Defected ground plane with three different sizes representing three different frequencies

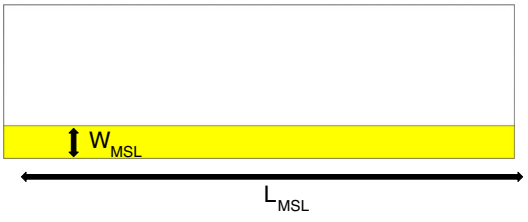

FIGURE 2 Top plane with a 50 Ω microstrip line

TABLE 1 Parameters for DGS bandstop design

a	b	c	d	e	f	g
7.5 mm	5 mm	5.4 mm	3 mm	8.5 mm	7.3 mm	3.5 mm
L	W	L_{MSL}	W_{MSL}	Cap_1	Cap_2	Cap_3
45 mm	15 mm	45 mm	3.2 mm	2.7 pF	8.2 pF	9 pF

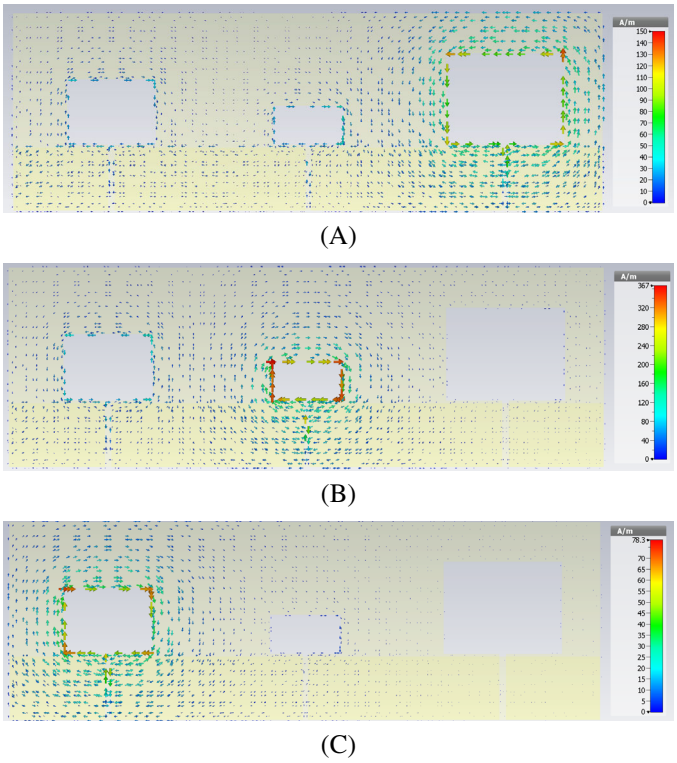

FIGURE 3 Surface current distribution: A, 433 MHz, B, 700 MHz, and C, 915 MHz

that the three cascaded sections largely work independently of each other and this can be observed in the surface current distributions provided in Figure 3.

2.2 | Multiband π-type equivalent circuit model

To validate the results of the tri-band DGS, a π-type circuit model is developed, using an earlier approach,[18] as shown in Figure 4. The inductor (L) and capacitor (C) combine to form the bandstop resonant frequency. A resistor (R) is introduced as part of the LC tank to model the dielectric losses. The parallel resistor-capacitor (R_pC_p)tank models the fringing fields at the discontinuity between the transmission line and DGS. Earlier work required all the ABCD parameters to obtain the various parameters of the circuit model. In this work, the calculation of just two of the ABCD parameters expressed in (2) to (3) are enough to get the required parameters. Moreover, the parameters of this equivalent circuit are calculated using the following equations.

$$R = \text{Real}(Z_{11}) \quad L = \frac{1}{4*\pi^2*f^2*C_{SMD}}, \tag{1}$$

$$A = \frac{[(1+S_{11})*(1-S_{11})]+S_{21}^2}{2*S_{21}}, \tag{2}$$

$$B = \frac{[(1+S_{11})*(1+S_{11})]-S_{21}^2}{2*S_{21}}, \tag{3}$$

$$Y_b = \frac{A-1}{B} \quad C_p = \frac{\text{Img}(Y_b)}{2*\pi*f} \quad R_p = \frac{1}{\text{Real}(Y_b)}. \tag{4}$$

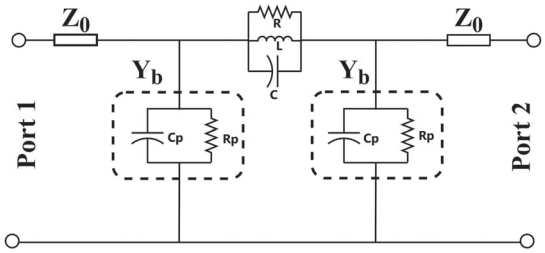

FIGURE 4 π-type equivalent circuit model for one band of the proposed BSF. BSF, bandstop filter

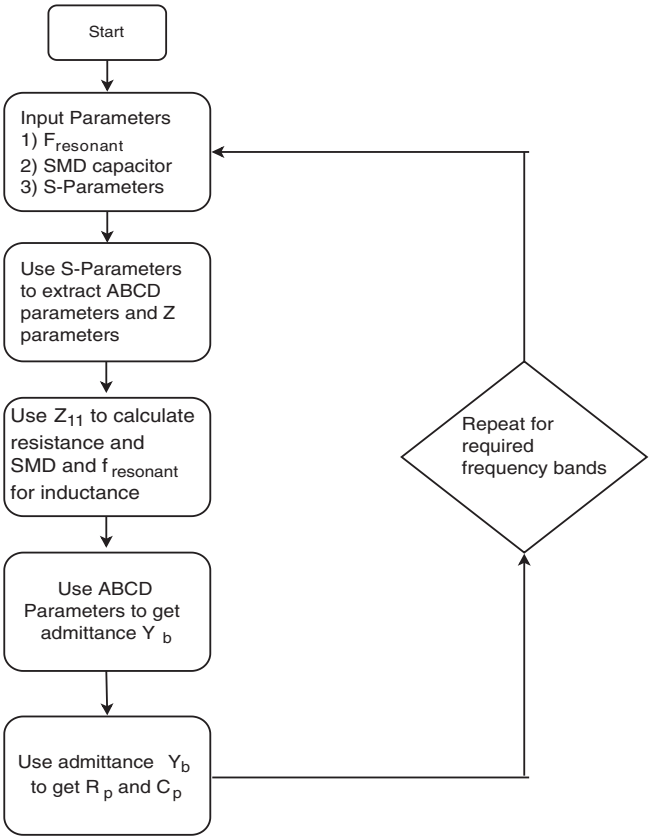

FIGURE 5 Flow chart depicting the multistopband filter design process

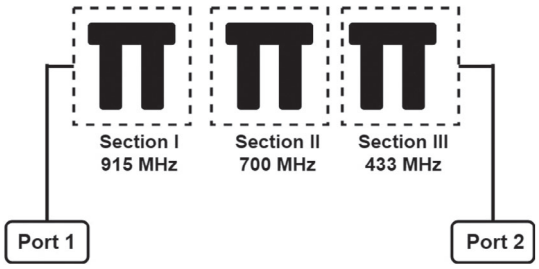

FIGURE 6 Cascaded tri-band filter using π type circuit model

The equivalent circuit is extended to a multiband model using the flowchart shown in Figure 5. In essence, the parameters of each resonant frequency are calculated in a loop. First, the S-Parameters are calculated from the EM simulation whose parameters are provided in Table 1. Then these parameters are used to extract the ABCD parameters. This in turn enable the calculation of all the parameters Y_b,C_p,and R_p.The resistance and inductance come from the Z-parameters and the resonant frequency found from the EM simulation.

The SMD capacitor and the resonant frequency aid in the calculation of the inductance The shape or size of the defect determines the inductance and therefore this circuit model would work for any defect shape or size. The circuit model is cascaded three times to accommodate the bandstop frequencies of 433, 700, and 915 MHz as shown in Figure 6. The relevant calculated parameters for the tri-band BSF are provided in Table 2.

TABLE 2 Parameters for triple-band circuit model

R_{915}	L_{915}	C_{915}	R_{p915}	C_{p915}
8400 Ω	11.2 nH	2.7 pF	294 Ω	0.55 pF
R_{700}	L_{700}	C_{700}	R_{p700}	C_{p700}
2000 Ω	6.3 nH	8.2 pF	33 Ω	0.23 pF
R_{433}	L_{433}	C_{433}	R_{p433}	C_{p433}
652 Ω	15 nH	9 pF	71 Ω	0.6 pF

3 | MEASUREMENT AND RESULTS

To validate the EM and circuit simulation, a prototype of the tri-band BSF, shown in Figure 7, is fabricated. This filter is connected by two ports and both these ports are connected to the defected ground and also to the 50 Ωmicrostrip line. The external SMD capacitors used and soldered on to the excitation slots of the semi-H shaped DGS are:

- 2.7 pF-Murata GJM Series (GJM1555C1H2R7WB01D)
- 8.2 pF-Murata GJM Series (GJM1555C1H8R2WB01D)
- 9 pF-Walsin MLCC (0402N9R0C500CT)

The prototype is characterized using Keysight E5063A VNA over a frequency range of 400 MHz to 1 GHz. The measured S-parameter results along with the CST simulation as well as ADS simulation are plotted in Figure 8. There are distinct three bandstop resonances apparent and all the three, namely, EM, circuit simulation and measurement results are in very good agreement.

There appears slight shift in the resonance frequencies and this can be attributed to the presence of the external SMD capacitors. These SMD capacitors although help in size reduction and are relatively easy to solder but suffer from poor tolerances. In brief, the shift in resonant frequencies can be overcome by using lower tolerance capacitors. Another solution is the tuning of the resonant frequency using a varactor diode. Furthermore, the rejection in the measured values is different when compared with the EM and circuit simulation values due to the soldering and connector losses. There are also radiation losses arising from the feedline being close to the edge of the PCB which can be resolved by designing the feedline toward the center of the structure rather than at edge.

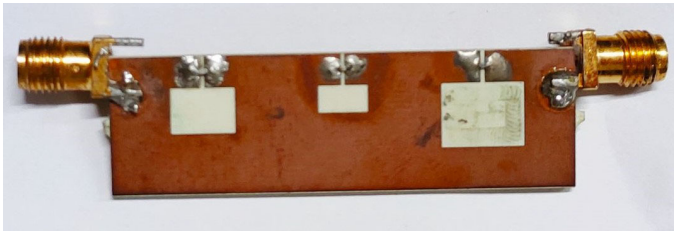

(A)

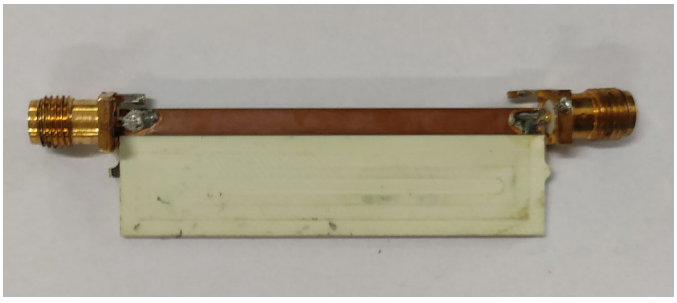

(B)

FIGURE 7 A, Ground plane with defect, B, Top plane with microstrip line

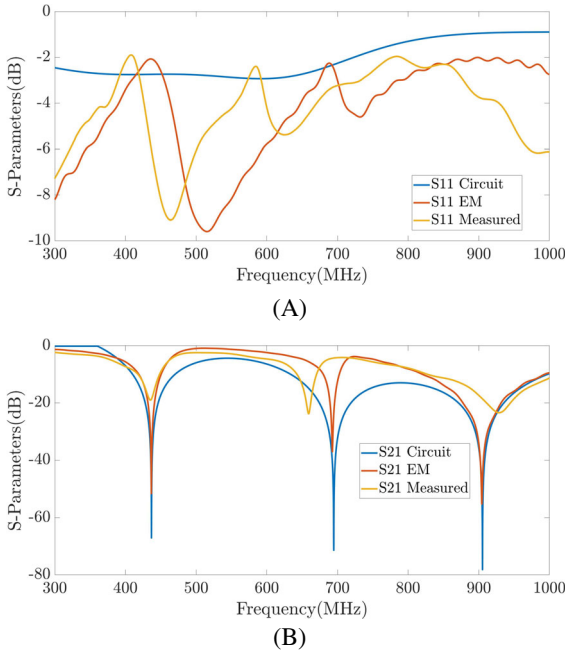

FIGURE 8 The *S*-parameters demonstrating a very good agreement between the EM, circuit simulation and measurement for the return loss and transmission: A, S11, B, S21

4 | BANDPASS FILTER

The second filter explored is the commonly used H-shaped DGS having a bandpass and bandstop response. The H shaped defect in the ground plane, shown here in Figure 9A, perturbs the 50 Ωmicrostrip transmission line to give rise to a stopband frequency. Now, in order to introduce a bandpass frequency, a gap in the feed line is introduced as shown in Figure 9B. Apparently there are two excitation slots which house two SMD capacitors. The first excitation slot is in the ground plane, having a length of L_2,that incorporates SMD capacitor Cap_1responsible for controlling the bandstop response. The other excitation slot, that is, the coupling gap, holds capacitor Cap_2responsible for controlling the bandpass response. A thorough EM simulation and optimization in CST is carried out and the resulting parameters needed to design this filter at a stopband frequency of 0.77 GHz and passband frequency of 0.70 GHz are provided in Table 3.

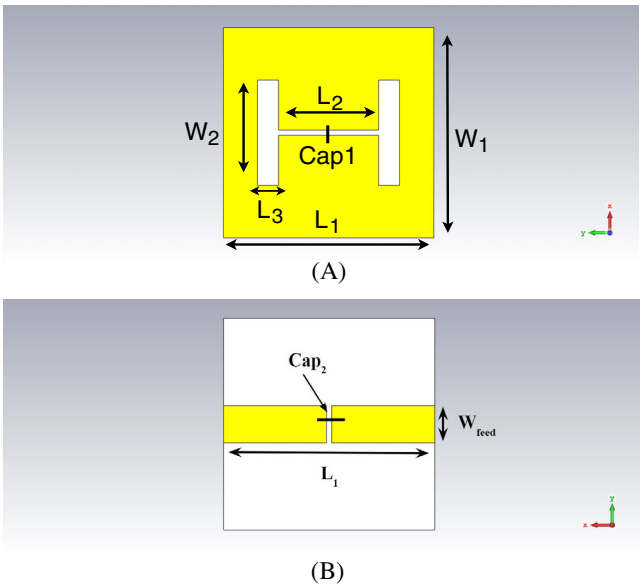

FIGURE 9 A, Ground plane with H-shaped DGS, B, Top plane with a 50 Ω feed line and a coupling gap. DGS, defected ground structures

TABLE 3 Parameters for EM simulation of filter

L_1	L_2	L_3	W_1	W_2	W_{feed}	Cap_1	Cap_2	Gap
20 mm	9.5 mm	10 mm	20 mm	2 mm	3.5 mm	9 pF	3pF	0.5 mm

FIGURE 10 π type circuit model for bandpass/bandstop filter

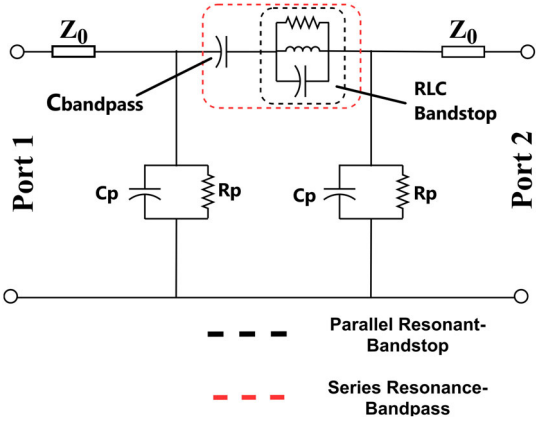

TABLE 4 Parameters for circuit design

L_{BSF}	R_{BSF}	C_{BSF}	R_p	C_p	C_{BPF}	L_{BPF}
4.74 nH	2000 Ω	9 pF	348 Ω	0.65	3 pF	16.5 nH

Abbreviation: BSF, bandstop filter, BPF, bandpass filter.

5 | NEW CIRCUIT MODEL

The equivalent inductance along with the coupling gap capacitance present in the microstrip feed line introduces a series resonance and hence an additional frequency response to the circuit. This additional frequency is the passband. The introduction of a series capacitor to the original circuit, shown in Figure 10, includes the modules responsible for the series and parallel resonances. Similar to previous section on triple-band filter, the circuit parameters are extracted from the EM simulation. The circuit model requires the value of L_{BSF}which is calculated using (1). The bandpass and bandstop frequencies are then extracted from the S-parameter simulations. Furthermore, the parallel RC combination used to model the fringing effects remain as part of the circuit. The circuit parameters obtained using the expressions (5) and (6)[23] are provided in Table 3

$$L_{BPF} = \frac{L_{BSF}}{1-\left[\frac{f_{BPF}}{f_{BSF}}\right]^2}. \tag{5}$$

$$C_{BPF} = \frac{25.33}{L_{BPF} * f_{BPF}^2}. \tag{6}$$

Furthermore, the choice of the stopband and passband frequencies has to be in a manner such that $f_{BPF} < f_{BSF}$.Anexample simulation is carried out in and the obtained relevant circuit parameters are provided in Table 4.

6 | MEASURED RESULTS FOR THE NEW DGS

The BPF is fabricated on a Rogers 4350B substrate having ϵ_r=3.66, the height of 1.52 mm and a loss tangent of 0.0037. The prototype in Figure 11 shows the top and the ground plane of the structure. In this case, a 9 pF external SMD capacitor (Walsin MLCC 0402N9R0C500CT) is soldered onto the gap in the DGS and the 3 pF external SMD capacitor (Murata GJM1555C1H3R0BB01D) is mounted in the coupling gap in the 50 Ωmicrostrip line. Two SMA connectors with impedance 50 Ωarealso soldered and then measurement is performed using a Keysight N9926A handheld VNA over a frequency range of 0.5 to 0.8 GHz.

The simulation results provided in Figure 12A clearly demonstrates the effectiveness of the proposed equivalent circuit that models both the bandpass and bandstop behavior. The measured results given in Figure 12B shows the presence of a sharp bandstop and bandpass response and thus validates the effectiveness of the proposed design. However, some anomaly between the simulation and measurement can be seen considering that the proposed design is also prone to port

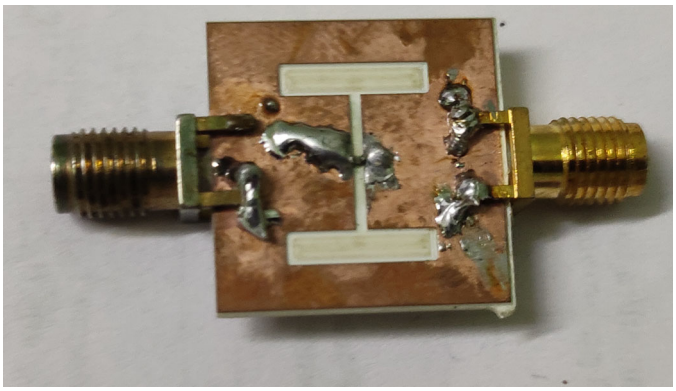

(A)

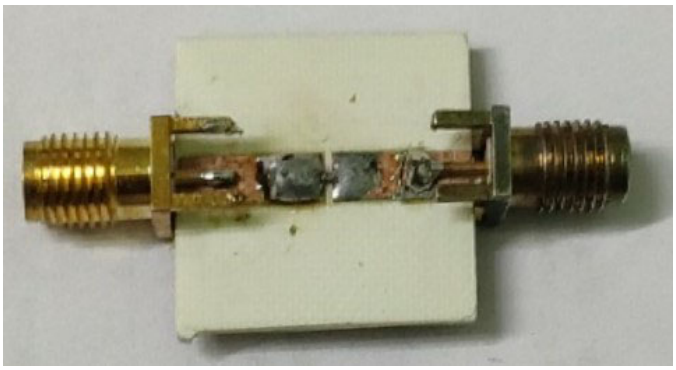

(B)

FIGURE 11 Fabricated H-shaped bandstop/bandpass filter, A, Ground plane, B, Top plane

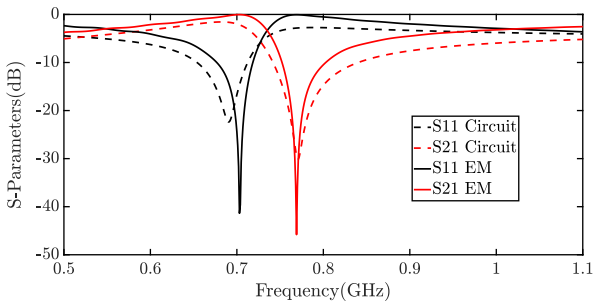

(A)

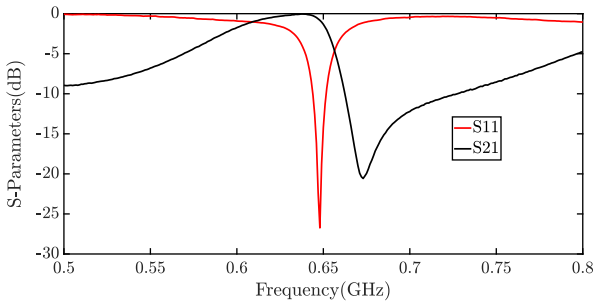

(B)

FIGURE 12 A, EM and circuit simulation, B, measured result of passband and stopband frequencies

or connector losses, in-house fabrication, and soldering issues. Another factor which influences the shift in frequency is the tolerance of the SMD. To avoid this, one can fabricate multiple prototypes until the desired frequency is achieved. Another route that can be explored is using capacitors with extremely low tolerances or utilizing a varactor diode for tuning the frequency.

7 | CONCLUSION AND FUTURE WORK

The design and analysis of two DGS-based filters has been presented in this article. Both designs revisit and utilize π-circuit model and improves the earlier reported equivalent RLC only model. It has been shown that the external SMD capacitors and the defect contribute to the LC tank which controls the resonant frequency. The improved πmodel accounts for the discontinuity present between the microstrip feed line and the defected ground plane. Both the designs are fabricated on Rogers 4350B substrate and the measured results are in very good agreement with their respective EM and circuit simulations and thus validate the proposed designs and analysis.

In future, this work can be further enhanced by utilizing printed or interdigital capacitors. This can remove the need for SMD capacitors which have tolerance issues. Another area of focus would be to explore the designs of multiband filter using DGS having both passband and stopband properties for miniaturized and compact size. This reduction in size can be used for emerging wireless applications.

PEER REVIEW INFORMATION

Engineering Reports thanks Luong Duy Manh and other anonymous reviewers for their contribution to the peer review of this work.

CONFLICT OF INTEREST

The authors have no conflict of interest related to this article.

AUTHOR CONTRIBUTIONS

Sambhav Malhotra contributed to conceptualization-lead, data curation-lead, formal analysis-lead, investigation-lead, methodology-lead. Mohammad Hashmi contributed to project administration-supporting, resources-supporting, software-supporting, supervision-supporting, validation-supporting, writing-original draft-supporting, writing-review and editing-supporting.

ORCID

Sambhav Malhotra https://orcid.org/0000-0003-0806-2081
Mohammad Hashmi https://orcid.org/0000-0002-1772-588X

REFERENCES

1. Verma S, Rano D, Hashmi MS. A novel miniaturized band stop filter using fractal type defected ground structure (DGS). Paper presented at: Proceedings of the 2017 IEEE Asia Pacific Microwave Conference (APMC); 2017:799-802.
2. Weng LH, Guo Y-C, Shi X-W, Chen X-Q. An overview on defected ground structure. *Progr Electromag Res*. 2008;7:173-189.
3. Verma S, Sareen E, Hashmi MS. A miniaturized dual-band right triangle defected ground structure band stop filter for energy harvesting applications. Paper presented at: Proceedings of the 2018 IEEE MTT-S International Microwave and RF Conference (IMaRC); 2018:1-3.
4. Ponchak GE. Dual of defected ground structure for coplanar stripline. *IEEE Microwave Wirel Compon Lett*. 2018;28(2):105-107.
5. Rano D, Hashmi M. Extremely compact ebg-backed antenna for smartwatch applications in medical body area network. *IET Microwave Antennas Propagat*. 2019;13(7):1031-1040.
6. Fan L, Qian HJ, Yangl B, Wang G, Luo X. Filtering power divider with wide stopband using open-stub loaded coupled-line and hybrid microstrip t-stub/DGS cell. Paper presented at: Proceedings of the 2018 IEEE/MTT-S International Microwave Symposium - IMS; June 2018:1-4.
7. Rao Y, Qian HJ, Yang B, Gómez-García R, Luo X. Dual-band bandpass filter and filtering power divider with ultra-wide upper stopband using hybrid microstrip/DGS dual-resonance cells. *IEEE Access*. 2020;8:23 624-23 637.
8. Mahmoud KR, Montaser AM. Design of compact mm-wave tunable filtenna using capacitor loaded trapezoid slots in ground plane for 5g router applications. *IEEE Access*. 2020;8:27 715-27 723.
9. Verma S, Rano D, Hashmi M, Bohara V. A high q dual e-shaped defected ground structure for wireless power transfer applications. Paper presented at: Proceedings of the 2018 Asia-Pacific Microwave Conference (APMC); 2018:1435-1437.

10. Malhotra S, Hashmi M. Near-field wpt using defected ground structures for uhf rfid applications. Paper presented at: Proceedings of the 2019 IEEE International Conference on RFID Technology and Applications (RFID-TA); September 2019:16-21.
11. Dautov K, Gupta R, Hashmi M. A performance enhanced dual-band wireless power transfer system for practical ism bands. Paper presented at: Proceedings of the 2019 IEEE Asia-Pacific Microwave Conference (APMC); 2019:1259-1261.
12. Verma S, Rano D, Hashmi M. A novel dual band defected ground structure for short range wireless power transfer applications. Paper presented at: Proceedings of the 2019 IEEE Wireless Power Transfer Conference (WPTC); 2019:188-191.
13. Dautov K, Hashmi M, Nauryzbayev G, Nasimuddin N. Recent advancements in defected ground structure based near-field wireless power transfer systems. *IEEE Access*. 2020;8 81298-81309. http://dx.doi.org/10.1109/ACCESS.2020.2991269.
14. Hekal S, Abdel-Rahman AB, Jia H, Allam A, Barakat A, Pokharel RK. A novel technique for compact size wireless power transfer applications using defected ground structures. *IEEE Trans Microwave Theory Techniq*. 2017;65(2):591-599.
15. Malhotra S, Verma S, Bohara V, Hashmi M. Dual-band wpt system using semi-h DGS for biomedical applications. Paper presented at: Proceedings of the 2019 IEEE Asia-Pacific Microwave Conference (APMC); 2019:720-722.
16. Barakat A, Yoshitomi K, Pokharel RK. Design approach for efficient wireless power transfer systems during lateral misalignment. *IEEE Trans Microwave Theory Techniq*. 2018;66(9):4170-4177.
17. Tahar F, Saad R, Barakat A, Pokharel RK. 1.06 fom and compact wireless power transfer system using rectangular defected ground structure resonators. *IEEE Microwave Wirel Compon Lett*. 2017;27(11):1025-1027.
18. Park J-S, Kim J-H, Lee J-H, Kim S-H, Myung S-H. A novel equivalent circuit and modeling method for defected ground structure and its application to optimization of a DGS lowpass filter. Paper presented at: Proceedings of the 2002 IEEE MTT-S International Microwave Symposium Digest (Cat. No.02CH37278); vol. 1, 2002:417-420.
19. Ren L. Tri-band bandpass filters based on dual-plane microstrip/DGS slot structure. *IEEE Microwave Wirel Compon Lett*. 2010;20(8):429-431.
20. Barakat A, Alshhawy S, Yoshitomi K, Pokharel RK. Triple-band near-field wireless power transfer system using coupled defected ground structure band stop filters. Paper presented at: Proceedings of the 2019 IEEE MTT-S International Microwave Symposium (IMS); June 2019:1411-1414.
21. Abdel-Rahman A, Ali AR, Amari S, Omar AS. Compact bandpass filters using defected ground structure (DGS) coupled resonators. Paper presented at: Proceedings of the IEEE MTT-S International Microwave Symposium Digest; June 2005:4.
22. Ahn D, Park C, Kim J, Qian Y, Itoh T. A design of the low-pass filter using the novel microstrip defected ground structure. *IEEE Trans Microwave Theory Techniq*. 2001;49(1):86-93.
23. Abdel-Rahman A, Verma AK, Boutejdar A, Omar AS. Compact stub type microstrip bandpass filter using defected ground plane. *IEEE Microwave Wirel Compon Lett*. 2004;14(4):136-138.
24. Chen Y, Liu C. Exploiting hi-lo inter-digital DGS for high-order microstrip bandpass filters. Paper presented at: Proceedings of the 2016 IEEE 5th Asia-Pacific Conference on Antennas and Propagation (APCAP); July 2016:83-84.
25. Ali M, Liu F, Watanabe A, et al. First demonstration of compact, ultra-thin low-pass and bandpass filters for 5g small-cell applications. *IEEE Microwave Wirel Compon Lett*. 2018;28(12):1110-1112.
26. Cui J, Chen L, Chang H, Sheng W. Compact ultra-wideband bandpass filter with configurable stopband based on diamond-shape resonator. *Int J RF Microwave Comput-Aid Eng*. 2020;30(1):e21996.
27. Boutejdar A. Design of 5 ghz-compact reconfigurable DGS-bandpass filter using varactor-diode device and coupling matrix technique. *Microwave Opt Tech Lett*. 2016;58(2):304-309.
28. Sengupta A, Roychoudhury S, Das S. Design of a miniaturized multilayer tunable super wideband BPF. *Progr Electromagnet Res*. 2020;99:145-156.
29. Cao X, Luo B, Zhu Y, Xia Z, Cai Q. Research on the defected ground structure with von Koch snowflake fractals. *IEEE Access*. 2020;8:32 404-32 411.

How to cite this article: Malhotra S, Hashmi M. Analysis of DGS filters using π-circuit model. *Engineering Reports*. 2020;2:e12196. https://doi.org/10.1002/eng2.12196